Journal of Alloys and Compounds 506 (2010) 263–267

Contents lists available at ScienceDirect

Journal of Alloys and Compounds

journal homepage: www.elsevier.com/locate/jallcom

Stability and electrical property of $Ba_{1-x}Sr_xCe_{0.8}Y_{0.2}O_{3-\delta}$ high temperature proton conductor

Siwei Wang[a], Fei Zhao[a], Lingling Zhang[a], Kyle Brinkman[b], Fanglin Chen[a,*]

[a] Department of Mechanical Engineering, University of South Carolina, 300 Main Street, Columbia, SC 29208, USA
[b] Savannah River National Laboratory, Aiken, SC 29808, USA

ARTICLE INFO

Article history:
Received 1 April 2010
Received in revised form 27 June 2010
Accepted 30 June 2010
Available online 7 July 2010

Keywords:
Barium cerate
Strontium cerate
Proton conductor
Electrical conductivity
Stability

ABSTRACT

The morphological and electrical properties of $Ba_{1-x}Sr_xCe_{0.8}Y_{0.2}O_{3-\delta}$ with x in the range from 0 to 1 prepared by a modified Pechini method were investigated as potential high temperature proton conductors. Dense microstructures were achieved for all the samples upon sintering at 1500 °C for 5 h. The phase structure analysis indicated that perovskite phase was formed for $0 \leq x \leq 0.2$, while for x larger than 0.5, impurity phases of Sr_2CeO_4 and Y_2O_3 appeared. The tolerance to H_2O for the samples improved with the increase in Sr content when exposed to boiling water, while the electrical conductivity decreased from $x = 0$ to 1. However, the resistance to CO_2 attack at elevated temperatures was not improved for $Ba_{1-x}Sr_xCe_{0.8}Y_{0.2}O_{3-\delta}$ within the whole x range studied.

1. Introduction

$SrCeO_3$ and $BaCeO_3$ based perovksite materials exhibit considerable proton conduction when doped with trivalent ions [1–4]. $SrCeO_3$ based electrolyte materials were first reported to possess predominately protonic conduction in atmospheres containing hydrogen or steam [1], while $BaCeO_3$ based materials may show mixed ionic (oxide ions and protons) conduction at elevated temperatures [5]. These high temperature proton conductors (HTPCs) can be used in applications for hydrogen gas sensors, hydrogen pumps, hydrogen membranes and especially for electrolyte materials for intermediate temperature (500–750 °C) solid oxide fuel cells (SOFCs) [6–8].

Many investigations have been made to improve the electrical conductivity of $SrCeO_3$ and $BaCeO_3$ based materials. Methods such as substituting isovalent and aliovalent ions into either A site or B site for the ABO_3 structure [9–14] may result in modified point defect concentrations which have impact on the electrical conductivity. In addition, materials synthesis using different preparation methods can affect the local stoichiometry and grain boundary interfaces resulting in conductivity modifications [15,16]. For example, $BaZr_{0.1}Ce_{0.7}Y_{0.2}O_{3-\delta}$ prepared by gel-casting technique has been reported to exhibit better sintering activity and higher electrical conductivity than that of the same composition prepared by solid-stated reaction method [17].

However, in certain applications such as the water gas shift reactions with gas phase carbon species present, the cerate perovskite structure is intrinsically unstable up to intermediate temperatures [18]. $BaCeO_3$ is a meta-stable state which can easily decompose to BaO and CeO_2 and is unstable upon exposure to CO_2 containing environment. For instance, $BaCe_{0.9}Y_{0.1}O_{2.95}$ will partially decompose during ageing in CO_2 atmosphere at 500 °C [19]. $SrCeO_3$ based materials also suffer from the issue of CO_2 attack to a lesser degree [20]. In addition, $SrCe_{0.95}Yb_{0.05}O_{3-\alpha}$ perovskite phase was reported to decompose under strongly reducing conditions such as dry H_2 at 1000 °C [21].

On the stability issue, many published papers have reported on the effect of doping ions into either B site or A site for the ABO_3 structure. Doping or co-doping into B site for $BaCeO_3$ and $SrCeO_3$ have proved to possess both high conductivity and good stability [22–25]. Kreuer et al. reported that it was possible to increase the lattice acidity and the chemical stability by partially replacing "B" site Ce^{4+} with more electronegative elements [26]. The introduction of Zr^{4+} ions into Ce sites to form $Ba(Ce_{1-x}Zr_x)O_{3-\delta}$ solid solution resulted in a favorable compromise between conductivity and stability [27]. For example, $BaZr_{0.1}Ce_{0.7}Y_{0.2}O_{3-\delta}$ has been reported to reach a conductivity of 0.03 S cm^{-1} at 700 °C in wet air while maintaining a pure phase perovskite structure under H_2 with 50 vol% H_2O at 750 °C for 300 h [28]. The chemical stability of $Sr(Ce_{1-x}Zr_x)_{0.95}Yb_{0.05}O_{3-\delta}$ ceramics against CO_2 attack has also been reported to improve with the increase in zirconium content: with Zr content increased to $x = 0.4$, the X-ray diffraction pattern of the ceramic did not change after the sample was exposed to 100% CO_2 atmosphere at 900 °C for 1 h [29].

* Corresponding author. Tel.: +1 803 777 4875.
E-mail address: chenfa@cec.sc.edu (F. Chen).

0925-8388/$ – see front matter © 2010 Elsevier B.V. All rights reserved.
doi:10.1016/j.jallcom.2010.06.188

The impact of A site doping on the conductivity and stability issues for $BaCeO_3$ based materials has also been reported. The cerate system $BaCe_{0.9}Nd_{0.1}O_{3-\delta}$ has been investigated by Yajima et al. by partially substituting Ca for Ba [13]. The oxygen ion conductivity decreased with increasing Ca content although the decrease in proton conductivity was insignificant. Hung et al. have recently reported that the chemical stability could be improved by small amount of A site Sr doping on $BaCe_{0.8}Y_{0.2}O_{3-\delta}$ [30]. They reported that $Ba_{0.9}Sr_{0.1}Ce_{0.8}Y_{0.2}O_{3-\delta}$ was more stable than $BaCe_{0.7}Zr_{0.2}Y_{0.1}O_{2.95}$ when exposed to a water vapor-rich environment. However, there seems to be some discrepancies with this conclusion. Regarding the stability test for the $BaCe_{0.7}Zr_{0.2}Y_{0.1}O_{2.95}$ material reported [31]. $BaCe_{0.7}Zr_{0.2}Y_{0.1}O_{2.95}$ was treated in boiling water; while the $Ba_{0.9}Sr_{0.1}Ce_{0.8}Y_{0.2}O_{3-\delta}$ material reported by Hung et al. [30] was exposed to a water vapor-rich environment at 80 °C. In liquid water, the kinetics of the decomposition of $BaCeO_3$ (doped or undoped) appears to be interface-controlled and is relatively fast. By contrast, in the presence of water vapor, the kinetics appears to be diffusion-controlled and is relatively sluggish [32]. Therefore the different experimental conditions utilized in literature reports on the stability of these materials have resulted in some confusion and a knowledge gap with regards to the stability of cerate perovskites under humid conditions.

This work aims to fill the knowledge gap and attempts to more completely understand the stability and the electrical properties of (Ba,Sr)(Ce,Y)$O_{3-\delta}$ materials. $Ba_{1-x}Sr_xCe_{0.8}Y_{0.2}O_{3-\delta}$ (BSCY, $x = 0$, 0.1, 0.2, 0.5, 1, denoted as BCY, BSCY1, BSCY2, BSCY5 and SCY, respectively) were prepared, the phase structure and chemical stability were investigated, and the electrical conductivities were evaluated in this work. The reactivity with water was evaluated in both liquid and gas phase conditions.

2. Experimental

2.1. Preparation

The $Ba_{1-x}Sr_xCe_{0.8}Y_{0.2}O_{3-\delta}$ powder was prepared by a modified Pechini method [33,34]. Starting materials $Ba(NO_3)_2$ (Alfa Aesar, 99.95%), $Sr(NO_3)_2$ (Alfa Aesar, 99%), $Ce(NO_3)_3{\cdot}6H_2O$ (Alfa Aesar, 99.5%) and $Y(NO_3)_3{\cdot}6H_2O$ (Alfa Aesar, 99.9%) were dissolved in deionized water and the nitrate concentration of the metal ions was determined through a titration method. Ethylenediaminetetraacetic acid (EDTA, Alfa Aesar, 99%) and citric acid (Alfa Aesar, 99%) were used as chelating and complexing agents, respectively, to which ammonium hydroxide (Sigma–Aldrich, NH_3 content 28.0–30.0%) was added to promote the dissolution of EDTA in deionized water. Stoichiometric amount of the metal precursors were then added into the chelating and complexing agents with citric acid:metal nitrates:EDTA molar ratio = 1.5:1:1.2. The solution was stirred at room temperature for 24 h, followed by heat treatment on a hot plate to obtain a brownish gel. The gel was then heated in a microwave oven to assist in drying and foaming. Subsequently, the dried ashes were heat-treated at 600 °C for 4 h in air to remove organic residue, followed by calcining at 1100 °C for 5 h in air with a heating rate of 3 °C min^{-1}. The obtained powders were pulverized with 8 wt% polyvinyl alcohol (PVA) binder and pressed into pellets under 400 MPa. The green pellets were then sintered at 1500 °C for 5 h in air.

2.2. Characterization

X-ray diffraction (XRD) patterns of the calcined and sintered samples were recorded on a X-ray diffractometer (Rigaku, Japan) with graphite-monochromatized Cu Kα radiation ($\lambda = 1.5418$ Å) using a scanning rate of 5 °C min^{-1} in the 2θ range from 20 to 80°. The structure and morphology of the synthesized products were characterized by scanning electron microscopy (SEM, FEI Quanta and XL 30) equipped with an energy dispersive X-ray spectroscopy (EDX) analyzer. For stability tests, sintered samples were exposed either to boiling water or to CO_2 atmospheres. After exposure, XRD patterns of the surface of the samples were collected and analyzed. For conductivity measurement, both sides of the sintered pellets were polished, painted with platinum paste, and heat-treated at 950 °C for 30 min prior to the electrical conductivity measurement. Platinum wires were attached to the surface of pellets. Electrical conductivity tests were conducted using AC impedance spectra with AC amplitude of 10 mV on a potentiostat/galvanostat with built-in impedance analyzer (Versa STAT3-400, Princeton Applied Research) in the frequency range of 0.1 Hz to 1 MHz at the temperature range of 450–800 °C.

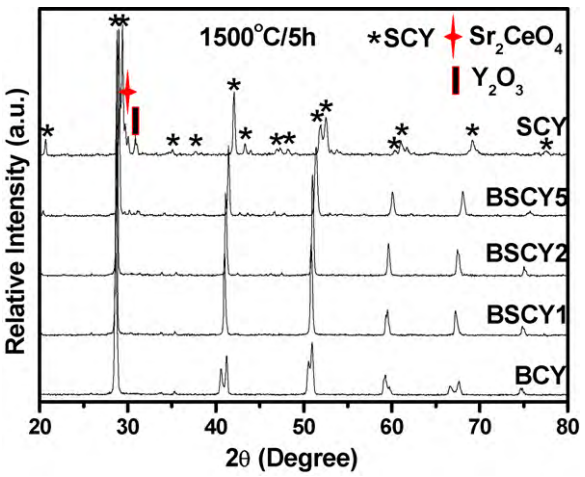

Fig. 1. XRD patterns of $Ba_{1-x}Sr_xCe_{0.8}Y_{0.2}O_{3-\delta}$ (BSCY, $x = 0$, 0.1, 0.2, 0.5 and 1, denoted as BCY, BSCY1, BSCY2, BSCY5 and SCY, respectively) sintered at 1500 °C for 5 h in air.

3. Results and discussion

3.1. XRD analysis

Fig. 1 shows the XRD patterns of the BSCY samples sintered at 1500 °C for 5 h. It can be seen that predominant perovskite structure is formed for all the samples. However, secondary phases such as Sr_2CeO_4 and Y_2O_3 appear for higher Sr content since the solubility limit of Y in $SrCeO_3$ is less than 20% [35,36]. It is also noted that the XRD peaks split for BCY, probably due to structure changes in the perovskite phase [37]. With the increase in Sr content, the diffraction peaks shifted towards larger diffraction angles indicating a decrease in the lattice parameter. This can be easily understood by the fact that the radius of Sr^{2+} (1.12 Å) is smaller than that of Ba^{2+} (1.35 Å). After substituting Ba^{2+} with Sr^{2+}, the lattice parameter decreases, resulting in shift towards larger diffraction angles.

3.2. Microstructure

The microstructures of the sintered samples are shown in Fig. 2. The graphs marked with “BCY”, “BSCY1”, “BSCY2”, “BSCY5” and “SCY” are the cross-sectional images for the samples. The graph marked with “SCY Surface” is a surface image for the SCY sample. It can be seen from the cross-sectional views of the samples that all the sintered samples formed dense structures. Archimedes’s water displacement measurements on the sintered disks indicate that all the sintered samples have relative densities greater than 95% of the theoretical values.

For samples BSCY5 and SCY, it is noticed that some small particles with an average grain size of about 2 μm exist, indicating the formation of secondary phases. Surface morphology for sample SCY is presented in Fig. 2 and EDX patterns for selected area A (representing large grain sizes) and B (representing small grain sizes) are shown in Fig. 3(a) and (b), respectively. It is difficult to identify the highest EDX peak of Sr from that of Y in Fig. 3. However, when the relative EDX peak intensity for Sr and/or Y with Ce is compared in Fig. 3(a) and (b), it can be seen that the relative Sr and/or Y content is higher in Fig. 3(b) (small grain sizes) than that in Fig. 3(a) (big grain sizes). Based on the XRD result for SCY, it is reasonable to conclude that the big grains are $SrCe_{0.8}Y_{0.2}O_3$ while the small particles are either Sr_2CeO_4 or Y_2O_3. Similar results also exist in sample BSCY5. The results would suggest that the solubility of Y in $BaCeO_3$ was larger than that in $SrCeO_3$, consistent with previous observations [35,36].

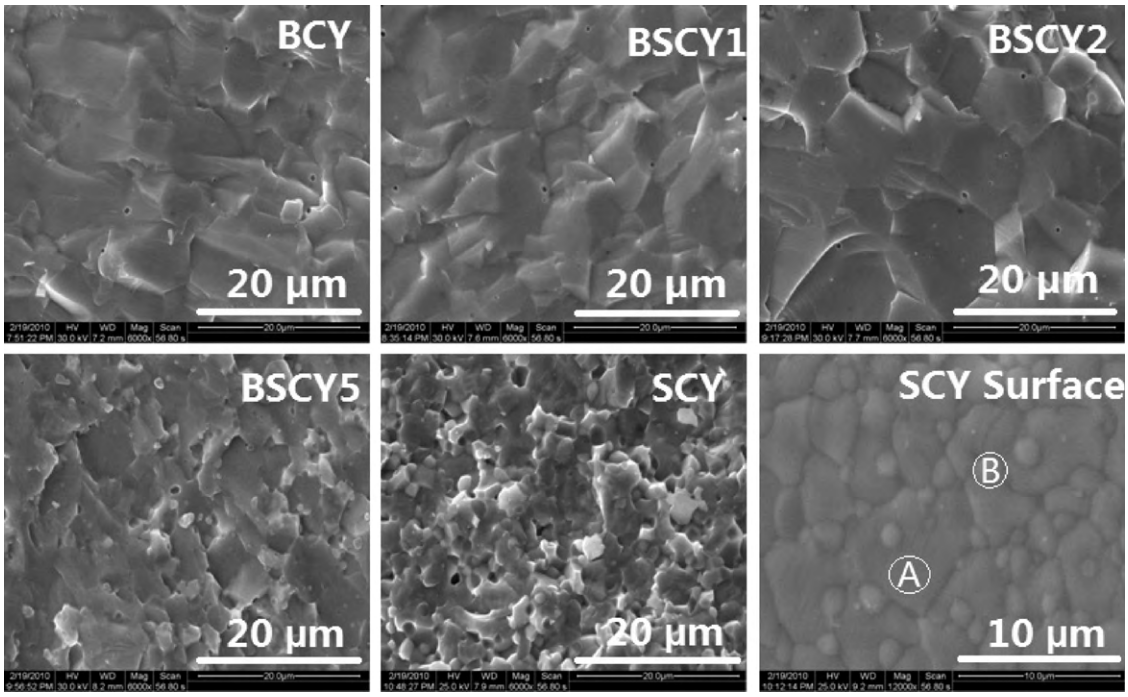

Fig. 2. The cross-sectional views of the BSCY sample pellets and the surface view of SCY sintered at 1500 °C for 5 h.

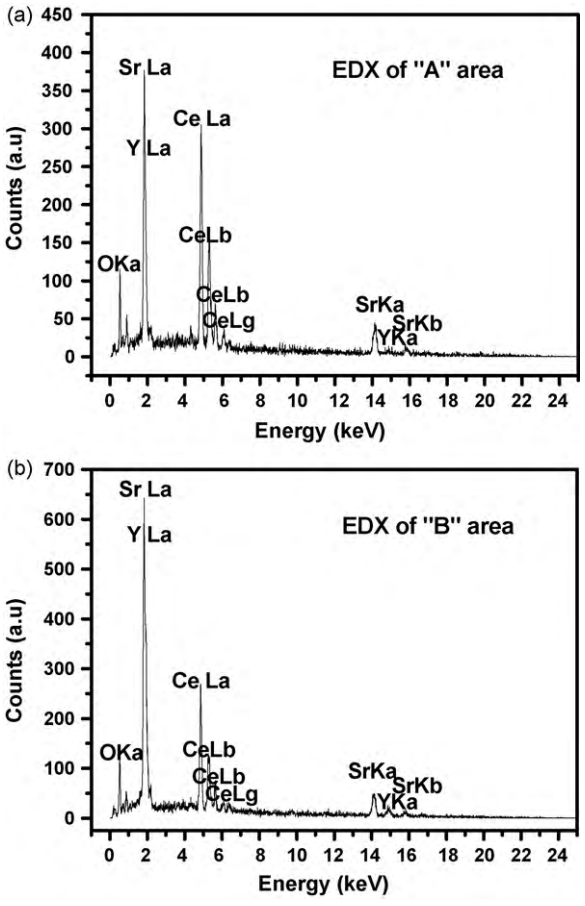

Fig. 3. EDX patterns for selected areas in SCY Surface shown in Fig. 2: (a) EDX of area A (representing large grain sizes) and (b) EDX of area B (representing small grain sizes).

3.3. Chemical stability

It has been demonstrated that $BaCeO_3$ is thermodynamically unstable in a water-containing atmosphere at elevated temperatures with the following decomposition reaction [19]:

$$BaCeO_3 + H_2O \rightarrow Ba(OH)_2 + CeO_2 \quad (1)$$

Thermodynamic calculation was conducted using HSC Chemistry Process Calculation Software [38]. Our thermodynamic calculation results on Gibbs free energy change, ΔG for reaction (1) also indicate that $BaCeO_3$ is thermodynamically unstable below 450 °C (shown in Fig. 4). Some doped $BaCeO_3$ based materials, such as 20 mol% Gd-doped $BaCeO_3$, were shown to be stable in water vapor at 600 and 700 °C for 1000 h but were unstable when heated in liquid water at 85 °C [39]. When considering the stability test, it is thus necessary to explore the possible effect of the sample treated in water vapor at high temperature, as well as treated at low temperature. Hung et al. have recently reported that $Ba_{0.9}Sr_{0.1}Ce_{0.8}Y_{0.2}O_{3-\delta}$ is kinetically stable in water rich envi-

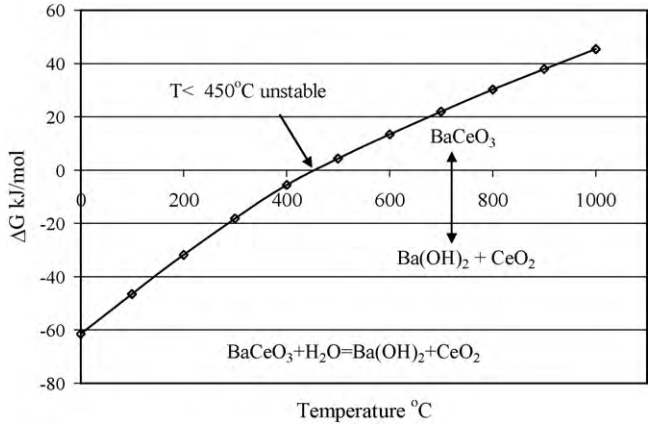

Fig. 4. Thermodynamic calculations on Gibbs free energy change as a function of temperature for reaction $BaCeO_3 + H_2O \rightarrow Ba(OH)_2 + CeO_2$.

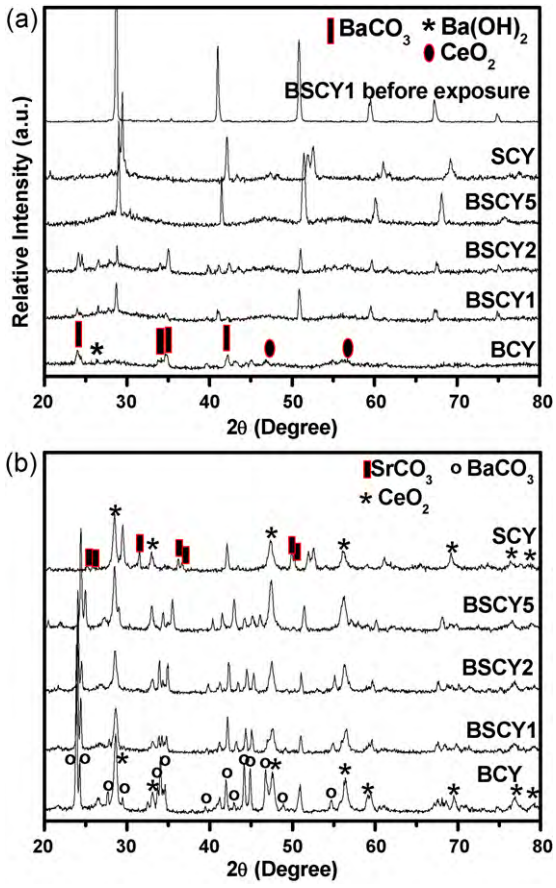

Fig. 5. (a) XRD patterns of the sintered BSCY pellets after exposure in boiling water for 4 h and (b) XRD patterns of the sintered BSCY pellets after exposure in wet CO_2 at 700 °C for 12 h.

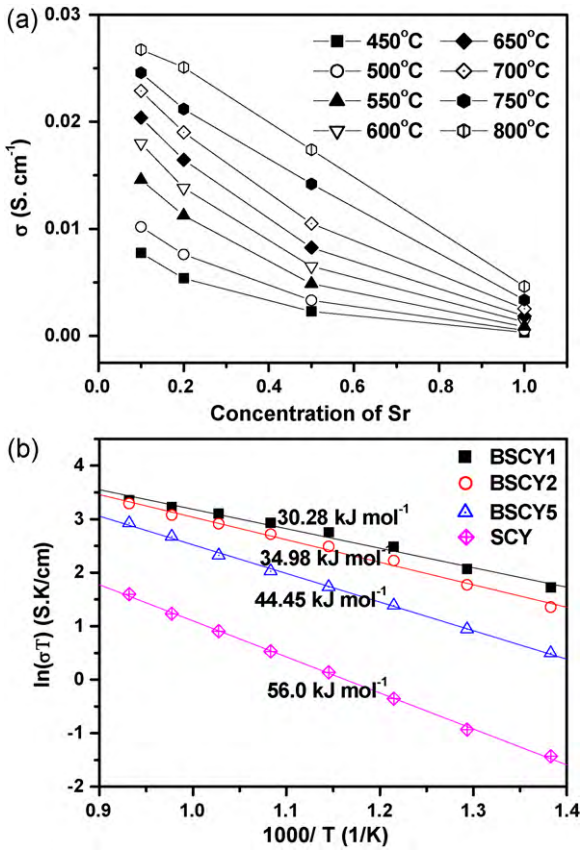

Fig. 6. (a) Electrical conductivities in wet H_2 atmosphere for BSCY samples as a function of Sr concentration measured at different temperatures and (b) Arrhenius plots of the electrical conductivities for BSCY samples in wet H_2 atmosphere.

ronment at 80 °C. This information, however, is not definitive to conclude that $Ba_{0.9}Sr_{0.1}Ce_{0.8}Y_{0.2}O_{3-\delta}$ is stable in heated liquid water. The mechanism for $BaCeO_3$ based material to react with water can be understood in Eq. (1). When $BaCeO_3$ based material is submerged in liquid water, the reaction product $Ba(OH)_2$ is soluble in water (though the solubility is modest), and the reaction product CeO_2 is insoluble, forming a porous layer on the surface of the $BaCeO_3$ based material. Further, the formation of $Ba(OH)_2$ can result in a substantial volume expansion, resulting in the formation of cracks in the surface of the $BaCeO_3$ based material. The subsequent water penetration into the material will occur via the cracking path and through the porous CeO_2 layer to react with the remaining $BaCeO_3$ [32]. However, in the presence of water vapor, after water reacting with a few surface monolayers of $BaCeO_3$, since fewer water molecules penetrate into the grain boundaries compared with those in liquid water environment, the dissolution of $Ba(OH)_2$ in water vapor would be very slow, and the subsequent reaction rate for the forward direction of reaction (1) would be expected to be much slower than that in liquid water. Consequently, the two sets of data obtained by Hung et al. [30] and Zhong [31] cannot be directly compared.

To evaluate the stability of BSCY in boiling water, sintered pellets with different contents of Sr were tested in boiling water for 4 h. Fig. 5(a) shows the XRD patterns of the pellets after treated in boiling water. For comparison, the XRD pattern of BSCY1 before exposure to boiling water was presented in Fig. 5(a). It can be seen from Fig. 5(a) that the XRD pattern for BCY changed significantly after treatment. After boiled in water for 4 h, BCY pellet, at least on the surface of the sample, reacted with H_2O and CO_2 to form $Ba(OH)_2$, CeO_2 and $BaCO_3$, as indicated in Fig. 5(a). The formation of $Ba(OH)_2$ and CeO_2 can be understood by Eq. (1), and the formation of $BaCO_3$ may be attributed by the reaction of $BaCeO_3$ with CO_2 dissolved in water or from air. Such impurity peaks could also readily be indexed for BSCY1 and BSCY2. For BSCY5 and SCY, however, these impurity peaks are insignificant, or at least not strong enough to be indexed. In other words, for BSCY samples with higher Sr content, the stability in water is enhanced. It can also be concluded from Fig. 5(a) that when placed in boiling water, $SrCe_{0.8}Y_{0.2}O_{3-\delta}$ will be more chemically stable than $BaCe_{0.8}Y_{0.2}O_{3-\delta}$.

The stability tests in carbon dioxide atmosphere at 900 °C for 2 h and in wet 3 vol% CO_2 (air as the balance gas, 3 vol% H_2O) at 700 °C for 12 h, respectively, were conducted to determine the stability of BSCY in CO_2 containing atmospheres. Fig. 5(b) shows the XRD patterns of the sintered BSCY pellets after exposure to wet CO_2 at 700 °C for 12 h. The XRD diffraction peaks after the CO_2 stability testing indicated that all the samples reacted with CO_2, with no observable reaction preference to either BCY or SCY. Based on chemical stability of BCY and SCY in CO_2, it is unlikely to expect that any composition of the mixture of BCY and SCY would be resistant to reactions with CO_2 at elevated temperatures.

3.4. Conductivity

Electrical conductivity data of the samples in wet H_2 in the temperature range of 450–800 °C are shown in Fig. 6(a) and (b). Fig. 6(a) shows the conductivities of BSCY measured at different temperatures as a function of the Sr concentration. It can be seen that the conductivity drops with the addition of Sr^{2+} ions into the Ba sites. Given that the conductivity of doped $SrCeO_3$ is lower than that of doped $BaCeO_3$, it is not surprising that the introduction of Sr into

the latter should result in a reduction in its conductivity. Furthermore, secondary phases such as Sr_2CeO_4 and/or Y_2O_3 formed due to phase segregations, as presented above, would also adversely affect the total electrical conductivity. Fig. 6(b) presents the Arrhenius plot of the conductivities as a function of the testing temperature. The activation energies of the samples are 30.28, 34.98, 44.45 and 56.0 kJ mol^{-1} for BSCY1, BSCY2, BSCY5 and SCY, respectively. There is a clear trend that the activation energy increases with the increase in Sr content. The conduction phenomena in these materials may be explained by an appropriate defect model (here we use the Kröger–Vink notation). Oxygen vacancies are generated through yttria-doping of the cerate. Under humidified conditions, hydroxide species can be produced by the oxidation of water vapor as shown in reaction (2).

$$H_2O_{(g)} + O_O^{\times} + V_O^{\bullet\bullet} = 2OH_O^{\bullet} \quad (2)$$

Protons could then migrate by hopping from the $OH_O^{\bullet}$ site to oxide ion site at a normal lattice site nearby causing this material to exhibit the proton conductivity [35]. In the presence of hydrogen, hydrogen can react with oxide ions in the lattice, producing hydroxide groups and electrons as in reaction (3).

$$\frac{1}{2}H_2 + O_O^{\times} = OH_O^{\bullet} + e' \quad (3)$$

In the presence of oxygen, the conduction phenomena should depend on the partial pressure of oxygen. Under wet hydrogen environment, the oxygen partial pressure is relatively low and oxide ions may leave the lattice, creating oxygen vacancies and electrons as expressed in reaction (4) [40].

$$O_O^{\times} = \frac{1}{2}O_{2(g)} + V_O^{\bullet\bullet} + 2e' \quad (4)$$

Consequently, doped $BaCeO_3$ shows mixed protonic and electronic conductivity in wet H_2 [14,41], resulting in relatively lower activation energies. Further, BSCY samples with more Ba content will exhibit lower activation energy, consistent with the previous study [42]. The data for $BaCe_{0.8}Y_{0.2}O_{3-\delta}$ did not show this kind of tendency. This difference may be due to the fact that $BaCe_{0.8}Y_{0.2}O_{3-\delta}$ is not as stable as BSCY in water-containing atmospheres, thus leading to deterioration in conductivity when tested for extended period under high vapor pressure environment at elevated temperatures. Considering both the stability and the conductivity testing results, it can be concluded that BSCY50 is an optimum composition by balancing the stability and electrical conductivity.

4. Conclusions

$Ba_{1-x}Sr_xCe_{0.8}Y_{0.2}O_{3-\delta}$ powders have been synthesized using a modified Pechini method to introduce Sr into Ba sites. Phase analysis showed that Y_2O_3 and Sr_2CeO_4 existed for $Ba_{1-x}Sr_xCe_{0.8}Y_{0.2}O_{3-\delta}$ with higher concentration of Sr content, indicating that the solubility of Y in $BaCeO_3$ is higher than that in $SrCeO_3$. The stability tests indicated that the resistance to boiling water for $Ba_{1-x}Sr_xCe_{0.8}Y_{0.2}O_{3-\delta}$ was between that of $BaCe_{0.8}Y_{0.2}O_{3-\delta}$ and $SrCe_{0.8}Y_{0.2}O_{3-\delta}$. Contrary to the reported data, $Ba_{1-x}Sr_xCe_{0.8}Y_{0.2}O_{3-\delta}$ was chemically less stable than $BaCe_{0.7}Zr_{0.2}Y_{0.1}O_{3-\delta}$ when exposed to boiling water. Due to the tendency of the reaction with CO_2 for both $BaCe_{0.8}Y_{0.2}O_{3-\delta}$ and $SrCe_{0.8}Y_{0.2}O_{3-\delta}$, it was not surprising that $Ba_{1-x}Sr_xCe_{0.8}Y_{0.2}O_{3-\delta}$ was also not stable in CO_2 containing atmospheres. The conductivity tests indicated that $Ba_{1-x}Sr_xCe_{0.8}Y_{0.2}O_{3-\delta}$ possessed the electrical conductivity between $BaCe_{0.8}Y_{0.2}O_{3-\delta}$ and $SrCe_{0.8}Y_{0.2}O_{3-\delta}$. The conductivity decreased and the activation energy increased with the increase in Sr content in $Ba_{1-x}Sr_xCe_{0.8}Y_{0.2}O_{3-\delta}$.

Acknowledgements

The authors acknowledge gratefully the financial support of the Department of Energy Nuclear Energy University Program (NEUP) (award no. 09-510) and the SRNL LDRD program.

References

[1] H. Iwahara, T. Esaka, H. Uchida, N. Maeda, Solid State Ionics 3–4 (1981) 359–363.
[2] H. Iwahara, H. Uchida, K. Ono, K. Ogaki, J. Electrochem. Soc. 135 (1988) 529–533.
[3] J.H. Cheng, W.T. Bao, D.C. Zhu, C.G. Tian, Q.Y. Yin, M. Ding, J. Alloys Compd. 484 (2009) 317–321.
[4] C. Chen, G.L. Ma, J. Alloys Compd. 485 (2009) 69–72.
[5] H. Iwahara, Solid State Ionics 52 (1992) 99–104.
[6] K.D. Kreuer, S. Adams, W. Munch, A. Fuchs, U. Klock, J. Maier, Solid State Ionics 145 (2001) 295–306.
[7] F. Zhao, R.R. Peng, C.R. Xia, Mater. Res. Bull. 43 (2008) 370–376.
[8] B.C.H. Steele, A. Heinzel, Nature 414 (2001) 345–352.
[9] W.B. Wang, J.W. Liu, Y.D. Li, H.T. Wang, F. Zhang, G.L. Ma, Solid State Ionics 181 (2010) 667–671.
[10] J.C. Zhang, Z.Y. Wen, J.D. Han, Y. Liu, J.G. Wu, X.G. Xu, J. Alloys Compd. 473 (2009) 308–313.
[11] W.H. Yuan, L.L. Mao, L. Li, Chin. Chem. Lett. 21 (2010) 369–372.
[12] F.L. Chen, O. Toft Sørensen, G.Y. Meng, D.K. Peng, J. Eur. Ceram. Soc. 18 (1998) 1389–1395.
[13] T. Yajima, H. Iwahara, H. Uchida, Solid State Ionics 47 (1991) 117–124.
[14] K. Katahira, Y. Kohchi, T. Shimura, H. Iwahara, Solid State Ionics 138 (2000) 91–98.
[15] M. Amsif, D. Marrero-López, A. Magrasó, J. Peña-Martínez, J.C. Ruiz-Morales, P. Núñez, J. Eur. Ceram. Soc. 29 (2009) 155–162.
[16] D. Ding, W. Zhu, J.F. Gao, C.R. Xia, J. Power Source 179 (2008) 177–185.
[17] H.P. Ding, B. Lin, D.R. Fang, Y.C. Dong, S.L. Wang, X.Q. Liu, G.Y. Meng, J. Alloys Compd. 474 (2009) 364–369.
[18] C.W. Tanner, A.V. Virkar, J. Electrochem. Soc. 143 (1996) 1386–1389.
[19] N. Zakowsky, S. Williamson, J.T.S. Irvine, Solid State Ionics 176 (2005) 3019–3026.
[20] S. Gopalan, A.V. Virkar, J. Electrochem. Soc. 140 (1993) 1060–1065.
[21] S. Okada, A. Mineshige, A. Takasaki, M. Kobune, T. Yazawa, H. Matsumoto, T. Shimura, H. Iwahara, Z. Ogumi, Solid State Ionics 175 (2004) 593–596.
[22] L. Bi, S.Q. Zhang, S.M. Fang, Z.T. Tao, R.R. Peng, W. Liu, Electrochem. Commun. 10 (2008) 1598–1601.
[23] K. Xie, R.Q. Yan, X.Q. Liu, J. Alloys Compd. 479 (2009) L40–42.
[24] F. Zhao, Q. Liu, S.W. Wang, K. Brinkman, F.L. Chen, Int. J. Hydrogen Energy 35 (2010) 4258–4263.
[25] S.W. Tao, J.T.S. Irvine, Adv. Mater. 18 (2006) 1581–1584.
[26] K.D. Kreuer, Annu. Rev. Mater. Res. 33 (2003) 333–359.
[27] C. Zuo, S. Zha, M. Hatano, M. Uchiyama, M.L. Liu, Adv. Mater. 18 (2006) 3318–3320.
[28] L. Yang, S.Z. Wang, K. Blinn, M.F. Liu, Z. Liu, Z. Cheng, M.L. Liu, Science 326 (2009) 126–129.
[29] J.C. Zhang, Z.Y. Wen, J.D. Han, J.G. Wu, S.H. Huang, X.J. Zhu, J. Alloys Compd. 440 (2007) 270–275.
[30] I.M. Hung, H.W. Peng, S.L. Zheng, C.P. Lin, J.S. Wu, J. Power Sources 193 (2009) 155–159.
[31] Z.M. Zhong, Solid State Ionics 178 (2007) 213–220.
[32] S.V. Bhide, A.V. Virkar, J. Electrochem. Soc. 146 (1999) 2038–2044.
[33] W. Zhou, Z.P. Shao, W.Q. Jin, J. Alloys Compd. 426 (2006) 368–374.
[34] W. Zhou, R. Ran, Z.P. Shao, H.X. Gu, W.Q. Jin, N.P. Xu, J. Power Sources 174 (2007) 237–245.
[35] H. Iwahara, Solid State Ionics 86–88 (1996) 9–15.
[36] P. Pasierb, M. Wierzbicka, S. Komornicki, M. Rekas, J. Power Sources 173 (2007) 681–687.
[37] N. Bonanos, K.S. Knight, B. Ellis, Solid State Ionics 79 (1995) 161–170.
[38] HSC Chemistry: Outokumpu Research Oy, Finland, www.outotec.com/hsc.
[39] Z.L. Wu, M.L. Liu, J. Electrochem. Soc. 144 (1997) 2170–2175.
[40] N. Bonanos, B. Ellis, K.S. Knight, M.N. Mahmood, Solid State Ionics 35 (1989) 179–188.
[41] E. Fabbri, T.K. Oh, S. Licoccia, E. Traversa, E. Wachsman, J. Electrochem. Soc. 156 (2009) B38–B45.
[42] A.S. Nowick, Y. Du, K.C. Liang, Solid State Ionics 125 (1999) 303–311.